# Battery management system with testing protocols for kW-class vanadium redox flow batteries

Andrea Trovò
Department of Industrial Engineering
Interdepartmental Centre Giorgio Levi Cases for Energy Economics and Technology
University of Padua - Padova, Italy
andrea.trovo@unipd.it

Massimo Guarnieri
Department of Industrial Engineering
Interdepartmental Centre Giorgio Levi Cases for Energy Economics and Technology
University of Padua - Padova, Italy
massimo.guarnieri@unipd.it

***Abstract*— A Battery Management System (BMS) for a kW-class vanadium redox flow battery (VRFB) was developed and is reported in this paper. This kind of BMSs is intrinsically different from those of solid-state batteries, due to the very different battery operating principle. Such BMS was built entirely in-house around a desktop computer provided with LabVIEW software which results in an expandable and flexible system capable of providing the battery with SCADA functions. It acquires and processes all data generated by the thermo-fluid and electric sensors, which are necessary to carry out the subsequent analyses. Moreover, this BMS also creates the feedback signals for controlling every operation, including experiments such as polarization curves plotting and efficiency computation. As regards polarization curves, this algorithm implements an experimental protocol that allows to obtain such performance in reproducible conditions and possibly comparable with those of similar stacks. The efficiency computation algorithm computes the energy absorbed (or delivered) by the battery while acquiring and controlling all signals so as to ensure safe conditions. The management of signal between stack and BMS includes the galvanic insulation of cell and stack voltages, consisting of multiple opto-isolators and a DC/DC transformer.**

***Keywords*— *Energy storage, battery management system, redox flow battery, smart grids.***

## I. Introduction

Energy storage systems have a crucial importance for vast number of applications such as transport [1], [2] electric vehicles [3], [4] and micro/smart grids [5]–[7]. Energy storage is also essential to manage the daily fluctuations of power demand in the grids, while coping with the intermittence of renewable sources [8], [9]. Several storage technologies have been proposed and are investigated, in order to address these problems, including pumping hydro, flywheel [10], compressed-air energy storage, supercapacitors and electrochemical storage in large batteries [11]. Among the electrochemical technologies the redox flow batteries with particular regard to the all Vanadium Redox Flow Batteries (VRFBs) represent a highly promising option for stationary electrochemical energy storage. They present an intrinsic combination of advantages, including power/energy independent sizing, low environmental impact, good round-trip efficiency, high operational flexibility and long cycle life [12]. Unlike all other solid-state batteries, Redox Flow Batteries (RFBs) can conveniently provide a wide range of different services, such as frequency regulation, peak shaving, load levelling, emergency backup, energy buffer for electric vehicle recharging stations and uninterruptible power supplies (UPS). The principles of this technology are well known, but a lot of development is needed to achieve high-performance grid-scale systems [13] and the full potential of RFBs remains unrealized. The main objective of this work is reporting on the experimental activities developed on a kW-scale vanadium redox flow battery with focus on its advanced Battery Management System (BMS). The BMS of a RFB follows a different concept than that of a solid-state battery, e.g. Li-ion, due to the very different structure of such batteries. To the best of the authors' knowledge, very few works were published on BMSs for industrial scale VRFBs. Lawder et al. published a review on the state of the art of BMSs and pertinent models for vanadium redox-flow batteries and lithium-ion batteries [14]. König et al. presented the general structure of a BMS for VRFBs [15]. However, detailed descriptions of real BMSs for kW-class VRFBs are still missing. The BMS here presented has been developed in LabVIEW environment, in order to exploit its flexibility in meeting the experimental needs and to implement SCADA functions in the battery. In particular two different testing procedures will be described. Firstly, the algorithm and software architecture devoted to collect experimental data of the polarization curves, namely the plots of the stack voltage vs. current is presented. In large RFB stacks these curves need to be plotted by means of a specific protocol in order to establish the steady concentration gradients of reactants and products inside the electrodes, at every measured data of the same curve. This condition allows to compare the performance of similar stacks in standardized and reproducible conditions. Secondly, the algorithm computing the energy and the charge exchanged by the stack is described. These quantities are then used to compute the battery efficiencies, while continuing to acquire and control all the other signals. The paper is organized as follow. Section 2 describes the IS-VRFB test facility and its power management system (PMS), for which the BMS was developed. In Section 3 the software of the BMS is described in detail, including its sections for the polarization curves and efficiency. The possible use of this work in the design and testing of future large scale VRFB systems is outlined in the conclusion in Section 4.

## II. IS-VRFB

The IS-VRFB test facility is in operation at the Energy Storage and Conversion Lab of the University of Padua, to develop the technology of large VRFBs (Fig. 1) [16]. It is rated 9 kW/27 kWh and its stack, i.e. the power converter, follows a conventional bipolar plate (BP) configuration consisting of 40 cells connected electrically in series and hydraulically in parallel. Each cell has a 600-cm$^2$ active area and is made with a Nafion® 212 membrane, two 5.7 mm thick (after compression)

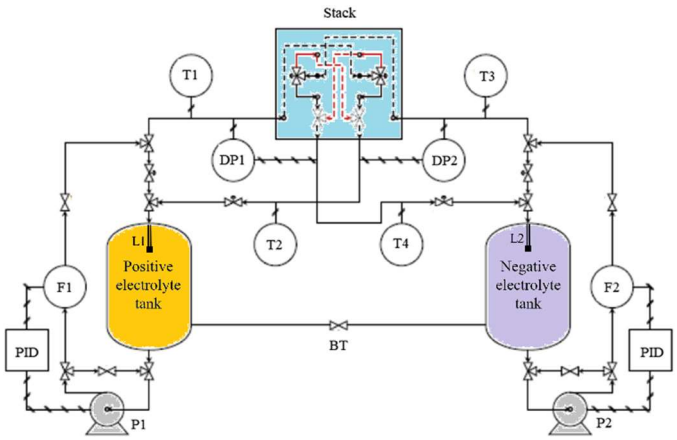


Fig. 1. IS-VRFB test facility and its main components: hydraulic circuits, stack, tanks, instrumentation: F1, F2: positive/negative electrolyte flow meter, L1/L2: positive/negative electrolyte level sensor, DP1/DP2 positive/negative electrolyte differential pressure meter. T1/T3: positive/negative electrolyte input temperature, T2/T4: positive/negative electrolyte output temperature, P1/P2 positive/negative electrolyte pump, BT by-pass tube.

graphite felt electrodes (Beijing Great Wall, China). Two closed hydraulic circuits circulate the vanadium ions 1.6 M solution in 4.5 M sulfuric acid between the stack and two 550-L tanks where energy is stored. The hydraulic circuits safe operation relies on monitored valves and interlock hardware/software logics. Two centrifugal pumps provide the needed electrolyte flow rates, being powered by two brushless motors controlled by two inverters which feedback modulate flow rates. The system is instrumented with level sensors, differential pressure probes, flow meters, and thermal transducers (RTDs). The electrical measurements are provided by 41 Alloy C276 rheophores for stack and cell voltages, a small cell, fed with the stack electrolytes, for Open Circuit Voltage (*OCV*), used to detect the battery state of charge (*SOC*), based on the Nernst law [17]. Two LEM current probes measure the stack current at low and high load, and a wattmeter measures the power supplied to the inverters which drive the pumps.

Power conditioning during charge/discharge is provided by the power supply (PS), that is an AC/DC bidirectional static converter remotely controlled by the BMS. This PS is complemented by a passive load (PL) for high current discharge tests. The PS is rated 0−85 V DC and ±75 A DC and its voltage/current profiles can be controlled at will. The BMS of IS-VRFB is capable of SCADA functions, i.e. it controls the battery operative variables (PS current and voltage and electrolyte flow rates) and also executes conditioning, logging and processing of all measurements and performs the subsequent analyses [18]. To this aim, all signals acquired by the sensors are received by a compact data acquisition device (Compact DAQ 9179 by National Instruments, NI US), which includes conditioning modules. Galvanic insulation between the IS-VRFB and Compact DAQ is ensured by opto-isolators (Isoblock by Verivolt, US) and by a DC/DC transformer (LEM CV 3-100/SP3) dedicated to the stack voltage signal.

## III. BMS - Software Architecture

The BMS consists of the Compact DAQ and of a desktop computer equipped with in-house software written in LabVIEW (NI). In this graphic programming environment, the software is built around a block diagram graphically composed in the front panel (the human-machine-interface, HMI) [18]. Specific functions are implemented by means of a number of tools and routines, dubbed *state machine*, *VI*, *SubVI*, *FIFO*, *cases*, *time structure*, *event case*, *error case structure, while loop, control loop, queue, wire, tdms (technical data management streaming)*, *front panel*…. The software of the IS-VRFB BMS was built making use of these LabVIEW tools and is structured in three main parts presented hereafter: Initialization, Error case structure, Final Sequence.

**Initialization**: in this part, the program runs some preliminary operations consisting of *VI* routines starting-up, Compact DAQ activation, and initialization of all Compact DAQ modules.

Here the code creates the *FIFO* queues that control the *state machines*, resets some residual values from previous experiments, and creates a path to the folder named with the current date where the experiment data are stored. All the *error wires* of this section govern the following *error case structure*.

**Error case structure**: if any error is generated in the initialization, this structure switches to *error case*, no further processing is performed and all variables are brought to the final sequence. If no error appears, the experiment program is enabled. This *case structure* consists of four *sub-structures*: a *while loop* named *UI Handling Loop*, a *control loop* with a *state machine* (*PFT Acquisition*), a simple *while loop* (*Voltage Acquisition Loop*), and a *state machine* (*Logging Loop*). This architecture allows to perform different operations simultaneously and independently as described hereafter.

*UI Handling Loop*: this *while loop* that includes an *event case*, allows modifying the sequence of the *state machines* by operating the related buttons in the *front panel*. The *event case* waits for a user-activated event, e.g. the arrest of the *PFT Acquisition* by operating the stop button in the *front panel*.

*PFT Acquisition*: this routine manages the acquisition of all signals from the battery: stack current, stack and cells voltages, electrolyte flow rates, electrolyte pressure drops, tank levels, electrolytes and room temperatures, and power consumption in the inverters (Fig. 2). The acquisition of most of these signals proceeds continuously while other functions can be activated.

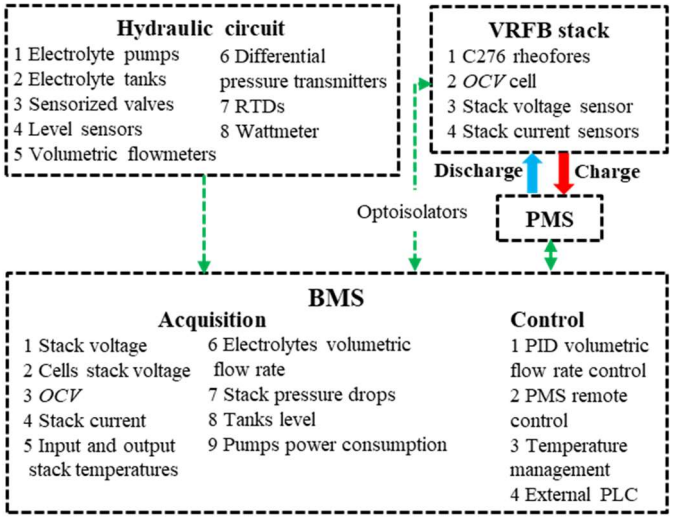


Fig. 2. Structure of the signals exchanged by the BMS

This routine consists of the following four subroutines.

Start and Acquisition (this is the default operation start): in this subroutine, LabVIEW acquires all experiment data from the battery and controls the electrolyte flow rates by sending PID signals to the inverters. The program stops when the user operates the *STOP button* on the *front panel*. In this subroutine the BMS also performs surveillance tasks, e.g. checking the status of valve microswitches, which are duplicated in an independent surveillance system built on a simple and robust PLC [16]. At any time, the user can decide whether to start or save any of the following three procedures by operating the pertinent buttons (Fig. 2).

Polarization curves: this subroutine creates and acquires automatically the experimental data which form polarization curves, according to defined experimental testing protocols [19], as described in the next Sub-section A.

Efficiency evaluation: this subroutine computes the energy exchanged by the battery during charge/discharge cycles [20–21], as described in detail in the next Sub-section B.

Temperature control: this subroutine activates a washing cycle whenever the RTD sensors measure stack electrolyte temperatures in excess of stated values which, particularly at high *SOC*, may trigger V(V) precipitation [17].

*Voltage Acquisition Loop*: this loop manages the acquisition of the cell voltages via the Compact DAQ modules. The voltage values are shown in the *front panel* as bar diagrams, to provide an immediate image of voltage unbalances.

*Logging Loop*: this is actually a user-operated *state machine* devoted to saving all data in a *tdms* files. It consists of four subroutines which regard: a) data received from the polarization subroutine; b) efficiency subroutine; c) manual data saving; d) data saving duration. The first two of them start automatically at the end of each process while the other two are activated by the user.

**Final Sequence**: in this phase all control outputs are set to zero and *queues* are emptied. All *tasks* are closed and, before the program stops, the error *wires* are connected and sent to a *VI* that displays possible error messages.

### *A. Polarization curves execution*

When a load is connected, a VRFB takes some time to reach the steady-state conditions which are maintained as long as the *SOC* start reducing significantly. If no galvanostatic control is applied in this transient phase after load connection an overcurrent appears which reduces and stabilizes at the steady-state value *I*. This behavior is related to the creation of concentration gradients of products and reactants inside the electrodes, after current insertion. Polarization curves were plotted using the PS remotely controlled by the BMS and the variable passive load at high current values. A LabVIEW procedure allows to plot automatically the curves by measuring the stack voltage at stack current increased in steps (Fig. 3). The procedure is parametrized for easy execution in different conditions (e.g. different *SOC* and flow rates). This procedure can constitute a standard protocol for performance assessment of other kW-class VRFBs. The procedure was implemented inside the "*PFT Loop*" and consisted of several cases inside a case structure.

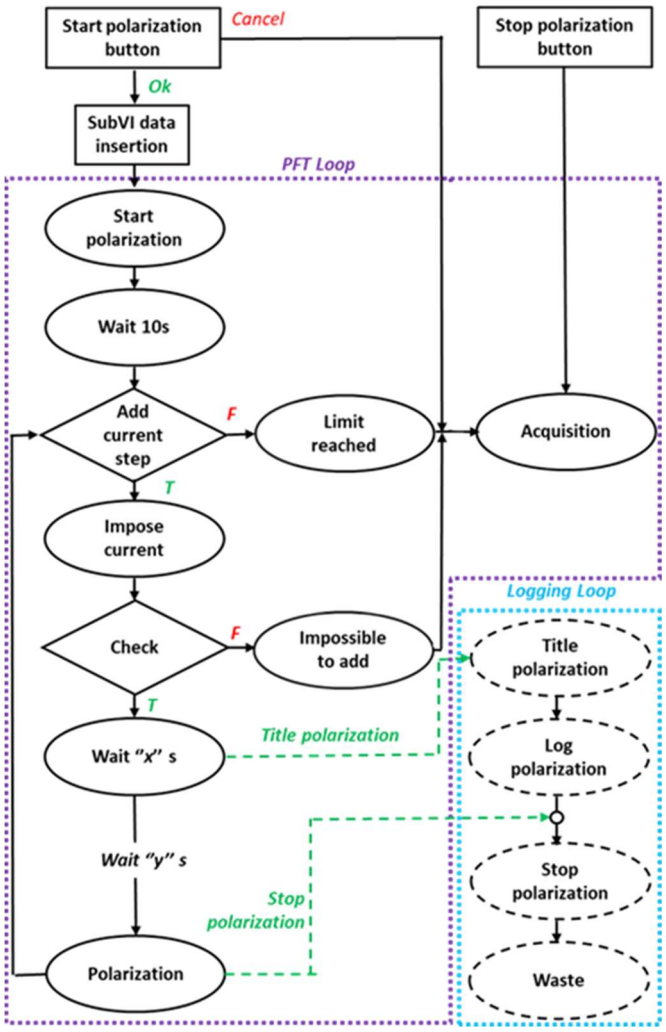


Fig. 3. Flowchart of the procedure collecting data for polarization curves drawing (green dotted lines indicate operator actions).

This subroutine consists of four main parts: the polarization logging folder path line, the start polarization and stop polarization buttons, and a LED labelled *processing*.

The folder indicator shows the path where the files are saved. The start button starts the experiment for plotting the polarization curve and the stop button stops the entire procedure at any point of the process. The *processing* LED is on while the process is running and, whatever event occurring in this period, it is going to be saved. Fig. 3 shows the flowchart of the procedure that collected and processed data.

When the *start polarization button* is operated, the program calls a *SubVI* named *polarization settings* that opens a support window where the user can choose between "charge" and "discharge" operation and set parameters such as flow rate, maximum PS voltage, current step, *SOC*, and current range. The *stop polarization button* causes the program return to the default acquisition case. The *start polarization button* confirms the inputted values and commands the procedure prosecution. The flowchart highlights the following actions.

- *Start polarization:* started by the *start polarization button*, sets the PS current to zero and the maximum PS voltage. Every time the current is increased by a step and the stack voltage

varies consequently, the user can check the actual values in the PS section on the *front panel*.

- *Wait 10 s*: stack powering is delayed by 10 seconds, to allows the cell voltages stabilizing after a previous operation.
- *Add current step*: in a preliminary step, the updated stack current setting is compared with the max current value to verify if the current limit has been reached. The result enters a *case structure*. If it is true, the loop continues, otherwise control moves outside the loop, as described hereafter.

- *False* (*limit reached*): this is the control that sets the current control to zero and takes the program to Start and Acquisition (default case). A message informs the user that the max current value has been reached and the acquisition of polarization curves data has ended.

- *True*: applies the updated setting to the current control.

- *Impose I*: the new current control value is sent on the power supply.
- *Check:* when the stack voltage reaches the inputted maximum PS voltage, the PS local logic limits the PS current to avoid exceeding such limit, as described hereafter in both true and false cases.

- *False* (*impossible to add*): in this condition the current control is set to zero and Start and Acquisition (default case) is started. A message shows that the current cannot be increased and the acquisition ends.

- *True*: the loop continues;

- *Wait "x"s*: the acquisition procedure is delayed for "*x*" seconds, to exclude fast insertion events (*x* can be selected according to the experimental needs, e.g. in the fast mode test it was set at 5 s as reported in [19]). In this period a logging file is created. Then, the logging loop starts.
- *Title polarization*: the values keyed by the user at the beginning of the procedure are assigned as the titles of the .xls file contained the polarization curve data.
- *Log polarization*: the stack voltage and current values are written in the new .xls file.
- *Stop polarization*: the procedure ends.
- *Polarization*: the program waits "*y*" seconds before stopping the logging loop and sending back the procedure to the *add current step* case. For example, this interval was set to 20 s in the fast mode operation on the IS-VRFB as reported in [19].

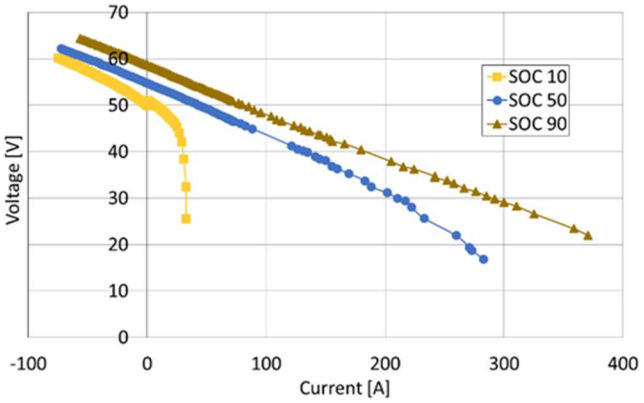


Fig. 4. IS-VRFB polarization curves during charging (negative current values)/discharging (positive currents values), collected through the polarization curves subroutines implemented on the IS-VRFB BMS.

When the procedure ends, data have been already stored in the logging file that is saved in a folder and is ready for the data post-processing. For the sake of completeness, the polarization curves during charging and discharging are reported in Fig.4 which are experimental collected through this subroutine implemented on such BMS. Further experimental results which make use of this subroutines are reported in [19].

### B. *Efficiency computation*

Several efficiency figures are considered to quantify the performance of IS-VRFB. Coulombic efficiency $\eta_C$ depends on the difference between stored and delivered charges due to the stack current $I(t)$:

$$\eta_C = \int_{dh} I(t)dt \Big/ \int_{ch} I(t)dt \tag{1}$$

Voltage efficiency $\eta_V$ depends on the differences in stack voltage $V(t)$ in charge and discharge due to cell overpotentials:

$$\eta_V = \int_{dh} V(t)dt \Big/ \int_{ch} V(t)dt \tag{2}$$

Round trip efficiency *RTE* depends on the energy losses during a charge/discharge cycle:

$$\begin{aligned} RTE &= [W - W_{an}]_{dh} \big/ [W + W_{an}]_{ch} \\ &= \int_{dh} [P(t) - P_{an}(t)]dt \Big/ \int_{ch} [P(t) - P_{an}(t)]dt \end{aligned} \tag{3}$$

where $P(t)=VI$ and $W$ are the electrical power and energy at the stack terminals; $P_{an}$ and $W_{an}$ are the power and energy supplied to the inverters of the hydraulic circuits. This *RTE* constitutes the most significant figure when considering a large-scale energy storage system for grid applications [21]. The implemented LabVIEW routine (Fig. 5) computes automatically the efficiency values according to previous expressions, based on the electric charges and energies exchanged by the stack, obtained by time integrating current and power while continuing acquiring and processing all other signals. This procedure can be controlled either manually or automatically. The program is designed to stop automatically as the desired *SOC* has been achieved or at any time by a user's action. The routine controls are placed in the efficiency window of the *front panel*. This routine consists of the following parts: the *start efficiency button* and *stop efficiency button*, which start or stop it; the *SOC* charge and *SOC* discharge numeric displays; a running timing indicator labelled *efficiency running time*, and a status window. Two numeric displays show the maximum and minimum *SOC* limits set by the user that are reached in a charge or discharge process. Two buttons activate the routine start or stop by sending a command to the *Handling Loop* section. When the start command is operated, LabVIEW launches a dedicated *SubVI* and a window opens. The user can set the following parameters: charge or discharge mode, stack current, *SOC* range, and maximum PS voltage. The local logic of the PS work as follows: once voltage and current are inputted, it operates as a constant current source until the battery voltage is smaller than the maximum PS voltage, otherwise it switches to voltage source reducing the current. Therefore, the charge (or the discharge) process is performed at constant current and then at constant voltage. The *start efficiency button* enters the inputted values as


Fig. 5. Flowchart of the section for the efficiency evaluations. The whole process is complicated by the presence of several security layers (the green dotted lines indicate the operator actions).

a *global variable,* whereas the *stop efficiency button* returns the program to the default acquisition mode.

This section is explained in detail hereafter.

- *Start efficiency*: starting time is recorded and memorized through a shift register. Buttons and windows are enabled or disabled. Stack voltage and current are taken from the *global variable* and are written on the respective internal controls. A preliminary check of the coherence of the *SOC* input values is made by comparing them with the actual *SOC* value (e.g. OK if the battery is lower than the charge target, ERROR in the opposite case; complementary conditions apply in discharge). If any error is detected, the routine switches to *error efficiency*, otherwise the efficiency acquisition process proceeds as follows.
- *Impose efficiency settings* the procedure sends the input current and voltage values to the power supply.
- *Efficiency*: this case is subdivided into two subcases: one for charge and one for discharge. Inside this case, some operations are performed continuously and others follow a sequential scheme. In particular, the pump control, which is ensured with proportional integral derivative (PID) algorithm, the computation of time integrals, and the running time, are independent of each other, so that they are performed every time the routine calls this case. The subcases are described hereafter:

- *SOC* < $SOC_{max}$*?*: this first case holds in charge and checks whether the input maximum *SOC* is larger than the current *SOC*. If this is true, the battery must be further charged and the procedure proceeds. Conversely, the charging process has been completed, the program switches to *finish efficiency* case and the collected data are stored. Complementary criteria apply in the case of discharge under the condition *SOC* > $SOC_{min}$.
- *Sign(I)>0?*: this intermediate case is necessary to detect possible errors in the PS operation. For example, if the user chooses the *Charge* setting but the PS works as an electronic load with *Sink* settings, the battery will never reach the input maximum *SOC,* even if this is larger than the current *SOC*. Depending on the operational mode of the PS (*charge* or *discharge*), the current must be positive or negative. Consequently, in the case of charge, if the current is positive no error occurs. Otherwise an error condition occurs. In the former case, further checks are carried out on the flow meter and the cells voltages inputs. As regards flow meters, the "true" output occurs when the flow is higher than the inputted value. As regards cells voltages, the "true" output occurs if none
- exceeds the value of 1.7 V. If these conditions hold, the procedure continues by returning to the *efficiency* case and repeating the double check procedure, otherwise, i.e. if just one of these conditions fails, PS current and voltage are set to zero and the routine proceeds to the *error efficiency* case. Complementary criteria apply in the case of discharge under the condition *sign(I)<0?*

During performing efficiency measurements, the battery controls prevent over-charging or over-discharging in order to avoid consequent issues, such as damages to the electrodes and formation of hydrogen [22].

When the *finish efficiency* string is sent in the *PFT loop queue*, the *start log efficiency* string is sent to the *Logging Loop* queue, on starting the procedure that saves the collected data in a *tdms* file.

- *Error efficiency*: this case shows two error messages to the user. One is a status string indicator in the *front panel* disappearing after some seconds that prompts the message: "incorrect set values – *SOC* is higher or lower than the current? Or the PS is working in incorrect mode". The second error message is a string indicator in the efficiency window of the *front panel* warning the user that "Error occurred, check settings or power supply mode." This message does not disappear until the *start efficiency button* is operated again, or the program is restarted, to allow for a longer check of the status of the efficiency routine. Even if any error occurs, the program automatically starts the procedure to save the data.
- *Finish efficiency*: this case allows storing the processed data inside the data saving *queue*, e.g. acquisition time, stack energy, hydraulic losses, stack current setting, initial and final *SOC* setting, exchanged charge, and voltage efficiency. Once completed, the program switches to the *prepare T control case* and the whole system is put in standby mode in which the electrolyte temperature is controlled, as stated above. Finally, the logging loop cycle goes to the *start save efficiency case*.
- *Start save efficiency*: in this *case*, the *tdms* file is created.
- *Save efficiency*: running time and all the energy data together with the current setting, the initial *SOC*, and the final *SOC* are written in the file.

• *Stop saving*: the data *queue* is emptied to avoid future overwriting and the *tdms* file is closed.

During the program execution the user can stop the acquisition and save the computed data at any time by operating the *stop efficiency button*; in this case the loop moves to the *finish efficiency case*.

For the sake of comparison, the results of the round-trip efficiencies (*RTE*) and energies computation is reported in Tab. 1. They were obtained through the efficiency subroutine implemented in this BMS on IS-VRFB. Tab.1 shows three *RTE* values at three different currents with a constant flow factor $\alpha$, which indicates the ratio between the electrical charges in the electrolyte flow and the electric current as described in detail in [23]. Further experimental results obtained with these subroutines are reported in [20], [21], [23].

TABLE. 1. EXPERIMENTAL ENERGY TERMS (*W*) AND ROUND-TRIP EFFICIENCIES (*RTE*) DURING CHARGE/DISCHARGE CYCLES AT CONSTANT CURRENT AND FLOW FACTOR α=8 [23].

| ***I*** | ***SOC range*** | $W_{ch}$ | $W_{dh}$ | $W_{an}$ | ***RTE*** |
|---|---|---|---|---|---|
| [A] | [%] | [Wh] | [Wh] | [Wh] | [%] |
| 30 | 13.1 – 87 | 17941 | 13610 | 1205 | 70.35 |
| 50 | 19.9 – 78.5 | 14273 | 10165 | 717 | 67.10 |
| 70 | 28.0 – 78.7 | 10809 | 7133 | 492 | 62.42 |

## IV. CONCLUSIONS

The BMS of a kW-class VRFB was developed in LabVIEW environment and successfully operated on the test facility. This paper presents its design and its software architecture. This BMS is capable of controlling the VRFB and its test programs with advanced strategies. It demonstrated its effectiveness and versatility in managing the experimental campaigns and in processing the large amount of data generated during the battery operation. The algorithms for generating the polarization curves and for computing the battery efficiency figures have been detailed. The first algorithm implements operative protocols ensuring repetitive sequences of load conditions, which can be parametrized to comply with regulatory standards which are under development [7]. The second algorithm ensures reliable efficiency computation. To the best of the author's knowledge, this is the first detailed description of a BMS for a large VRFB provided with advanced control strategies. A LabVIEW-based BMS like this can be quite easily replicated into a low-cost PLC-based BMS for commercial VRFBs applications.

## AKNOWLEDGMENT

This work was funded by the Interdepartmental Centre Giorgio Levi Cases for Energy Economics and Technology of University of Padua within the 2019 Project "Grid-optimized vanadium redox flow batteries: architecture, interconnection and economic factors" (GUAR_RICERCALASCITOLEVI 20_01).

## REFERENCES

[1] I. Perin, G. R. Walker, and G. Ledwich, "Load Sharing and Wayside Battery Storage for Improving AC Railway Network Performance, With Generic Model for Capacity Estimation, Part 1," IEEE Ind Electron, vol. 66, pp. 1791–1798, 2019.

[2] S. Vazquez, S. M. Lukic, E. Galvan, L. G. Franquelo, and J. M. Carrasco, "Energy Storage Systems for Transport and Grid Applications," IEEE Ind Electron, vol. 57, pp. 3881–3895, 2010.

[3] N. Li, F. Gao, T. Hao, Z. Ma, and C. Zhang, "SOH Balancing Control Method for the MMC Battery Energy Storage System," IEEE Ind Electron, vol. 65, pp. 6581–6591, 2018.

[4] W. Huang and J.A.A. Qahouq, "Energy Sharing Control Scheme for State-of-Charge Balancing of Distributed Battery Energy Storage System," IEEE Ind Electron, vol. 62, pp. 2764–2776, 2015.

[5] F.G. Torres, C. Bordons, and M.A. Ridao, "Optimal Economic Schedule for a Network of Microgrids With Hybrid Energy Storage System Using Distributed Model Predictive Control," IEEE Ind Electron, vol. 66, pp. 1919–1929, 2019.

[6] Y. Li, Z. Yang, G. Li, D. Zhao, and W Tian, "Optimal Scheduling of an Isolated Microgrid With Battery Storage Considering Load and Renewable Generation Uncertainties," IEEE Ind Electron, vol. 66, pp. 1565–1575, 2019.

[7] A. Lucas and S. Chondrogiannis, "Smart grid energy storage controller for frequency regulation and peakshaving, using a vanadium redox flow battery," Int J Elec Power, vol. 80, pp. 26–36, 2016.

[8] Y. Yang, Q. Ye, L.J. Tung, M. Greenleaf, and H. Li, "Integrated Size and Energy Management Design of Battery Storage to Enhance Grid Integration of Large-Scale PV Power Plants," IEEE Ind Electron, vol. 65, pp. 394–402, 2018.

[9] S.T. Kim, S. Bae, Y.C. Kang, and J.W. Park, "Energy Management Based on the Photovoltaic HPCS With an Energy Storage Device," IEEE Ind Electron, vol. 62, pp. 4608–4617, 2015.

[10] X. Li, B. Anvari, A. Palazzolo, Z. Wang, and Hamid Toliyat, "A Utility-Scale Flywheel Energy Storage System with a Shaftless, Hubless, High-Strength Steel Rotor," IEEE Ind Electron, vol. 65, pp. 6667–6675, 2018.

[11] L.Zhang, Y.Tang, S.Yang, and F.Gao"Decoupled Power Control for a Modular-Multilevel-Converter-Based Hybrid AC–DC Grid Integrated with Hybrid Energy Storage" IEEE Ind Electron, vol. 66, pp. 2926–2934, 2019.

[12] M. Guarnieri, P. Mattavelli, G. Petrone, and G. Spagnuolo, "Vanadium redox flow batteries: Potentials and challenges of an emerging storage technology," IEEE Ind Electron, vol. 4, pp. 20–31, 2016.

[13] L.F. Arenas, C. Ponce de León, and F.C Walsh, "Redox flow batteries for energy storage: their promise, achievements and challenges," Current Opinion in Electrochemistry, vol. 16, pp. 117–126, 2019.

[14] M.T. Lawder, B. Suthar, P.W.C. Northrop, S. De, C.M. Hoff, O. Leitermann, M.L. Crow, S. Santhanagopalan, and V.R. Subramanian, "Battery Energy Storage System (BESS) and Battery Management System (BMS) for Grid-Scale Applications," Proceedings of the IEEE, vol. 102, pp. 1014–1030, 2014.

[15] S. König and T. Leibfried, "Introduction of a Flow Battery Management System (FBMS)," Advanced Battery Power Conference 2015, Aachen, 2015, https://www.ieh.kit.edu/mitarbeiter_2306.php

[16] M. Guarnieri, A. Trovò, A. D'Anzi, and P. Alotto, "Developing vanadium redox flow technology on a 9-kW 26-kWh industrial scale test facility: Design review and early experiments," Appl Energ, vol. 230, pp. 1425–1434, 2018.

[17] A. Trovò, P. Alotto, M. Giomo, F.Moro, and M. Guarnieri, "A validated dynamical model of a kW-class Vanadium Redox Flow Battery," Mathematics and Computers in Simulation, doi:10.1016/j.matcom.2019.12.011, 2019.

[18] A. Trovò, "Battery management system for industrial-scale vanadium redox flow batteries: Features and operation," J Power Sources, vol. 465, 228229, 2020.

[19] M. Guarnieri, A. Trovò, G. Marini, A. Sutto, and P. Alotto, "High current polarization tests on a 9 kW vanadium redox flow battery," J Power Sources, vol. 431, pp. 239–249, 2019.

[20] A. Trovò, F. Picano, and M. Guarnieri. Maximizing, "Vanadium Redox Flow Battery Efficiency: Strategies of Flow Rate Control," 2019 IEEE 28th International Symposium on Industrial Electronics (ISIE), pp. 1977–1982, 2019.

[21] A. Trovò, F. Picano M. Guarnieri, "Comparison of energy losses in a 9 kW vanadium redox flow battery" J Power Sources, vol. 440, 227144, 2019.

[22] T. Jirabovornwisut and A. Arpornwichanop, "A review on the electrolyte imbalance in vanadium redox flow batteries," Int J Hydrogen Energ, vol. 44, pp. 24485–24509, 2019.

[23] M. Guarnieri, A. Trovò, and F. Picano, "Enhancing the efficiency of kW-class vanadium redox flow batteries by flow factor modulation: An experimental method," Appl Energ, vol. 262, 114532, 2020.